

Double-lined Spectroscopic Binaries from the LAMOST Low-resolution Survey

Junhui Liu^{1,2} , Bo Zhang³ , Jianfeng Wu¹ , and Yuan-Sen Ting^{4,5,2,6} 

Reporter: Zhang Xu

2025.5.9

1. Introduction

- ~50% of solar-type stars exist in binary or multiple-star systems
- Importance of studying binary systems:
 - Star formation and evolution
 - Compact object binaries and Type Ia supernovae
- Binary stars can be divided into visual binaries and spectroscopic binaries (SBs)
- SBs are further differentiated into single-lined binaries (SB1s) and double-lined binaries (SB2s)
- Few studies on SB2s in low-resolution spectra
- LAMOST LRS DR9: $R \sim 1800$, 11,226,252 spectra for 10,907,516 stars, 3700-9000Å

2. Methods

- **Data Preprocessing:**
 - g-band SNR ≥ 30
 - Removing high-temperature sources with $T_{\text{eff}} > 9000$ K using CCF(cross correlation functions)
 - 3,584,214 spectra, for 2,027,146 objects each with one single observation, and 592,622 objects with multiple observations

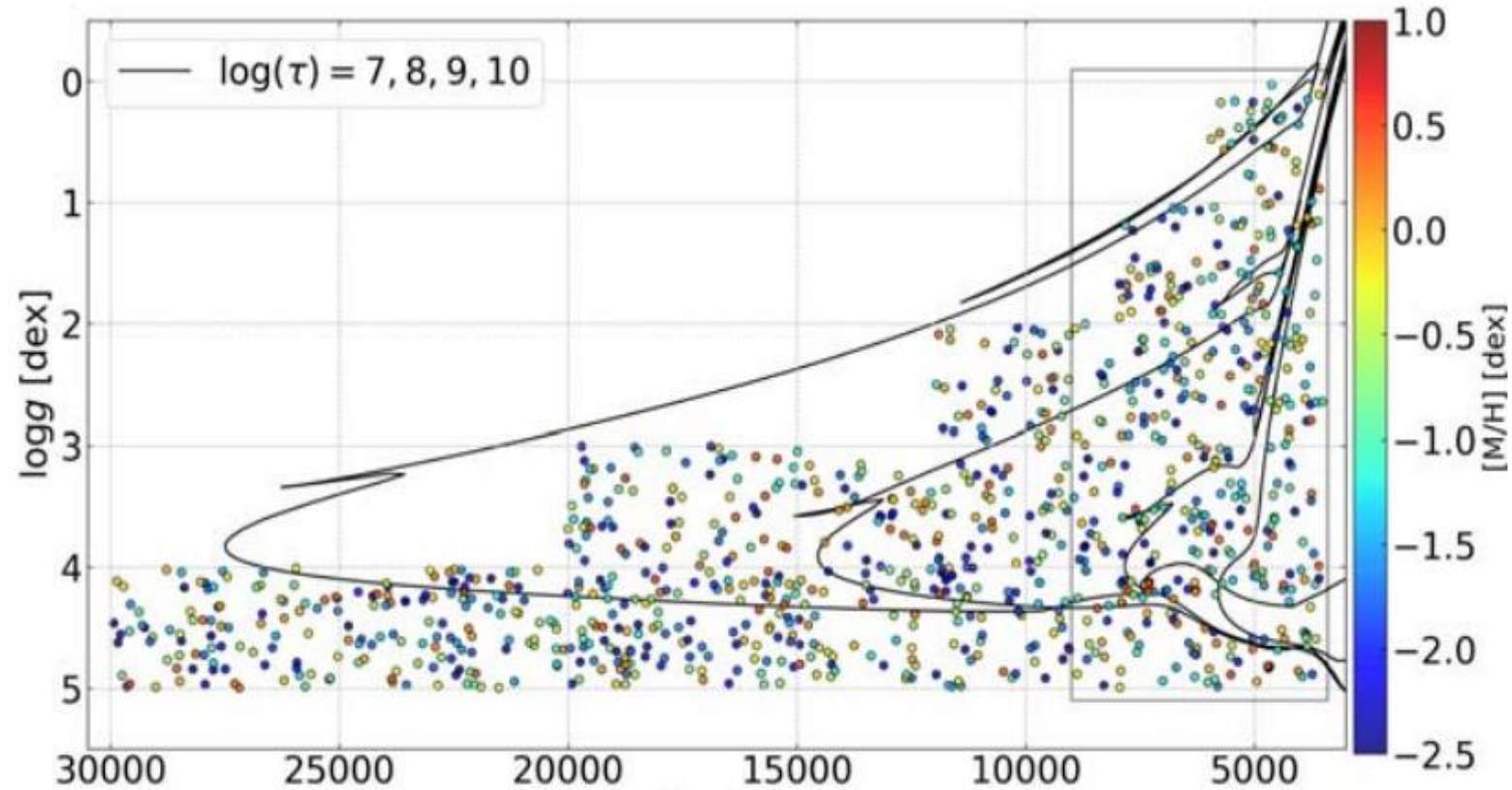


Figure 3. The distribution of T_{eff} , $\log g$, and $[M/H]$ of CCF template spectra. Superposed is a series of isochrones with solar metallicity but different ages τ in years. The gray box indicates the parameter space with $T_{\text{eff}} < 9000$ K left in the data preprocessing using the CCF method, which includes 405 template spectra.

2. Methods

- **Training Data Sample:**
 - Employing a crossmatch radius of 3" between the spectra of LAMOST LRS DR9 and spectral parameters of APOGEE catalogs and applying the following criteria:
 1. $3500 \text{ K} < T_{\text{eff}} < 8000 \text{ K}$,
 2. $0 < \log g < 5.0 \text{ dex}$,
 3. $-2.0 < [M/H] < 1.0 \text{ dex}$,
 4. $|V_{\text{APOGEE}} - V_{\text{LAMOST}}| < 50 \text{ km s}^{-1}$,
 5. "ASPCAPFLAG" = 0,
 6. the SNR of APOGEE spectra and that of LAMOST LRS DR9 at the g band are all greater than 30,
 - Finally, getting 74,768 objects as single star sample

2. Methods

- **Single-star Model:**
- **SLAM (Stellar Label Machine; B. Zhang et al. 2020a, 2020b)** used for training
- Input: Normalized LAMOST LRS DR9 spectra (3950-5750 Å)
- Parameter vector $\theta = \{T_{\text{eff}}, \log g, [M/H], [\alpha/M]\}$
- Iterative refinement process: 74,768 \rightarrow 64,013 training objects
- Parameter uncertainties: $\sigma(T_{\text{eff}}) = 61.76$ K, $\sigma(\log g) = 0.11$ dex, $\sigma([M/H]) = 0.05$ dex, $\sigma([\alpha/M]) = 0.03$ dex
- MIST stellar evolution model to convert mass, age \rightarrow atmospheric parameters

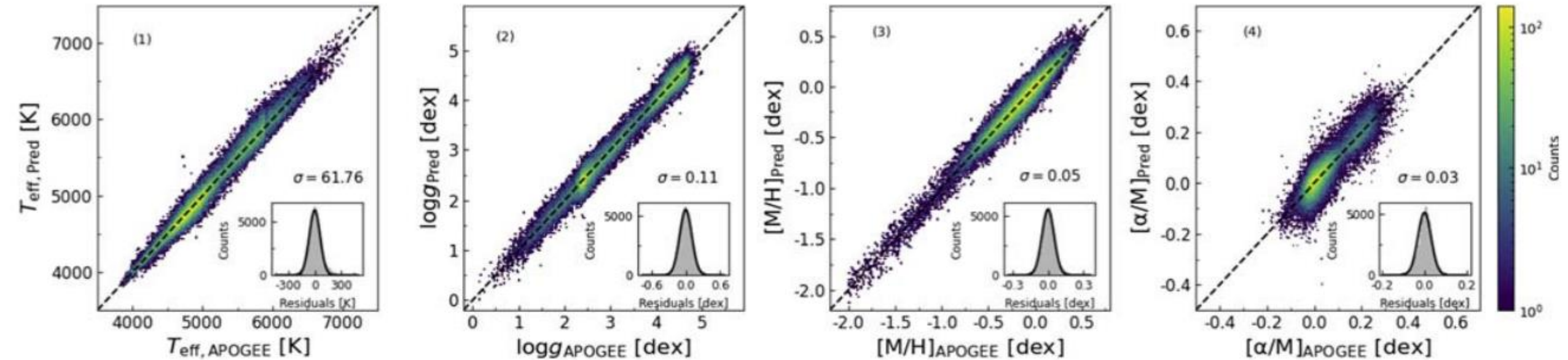


Figure 5. The comparison distributions of T_{eff} , $\log g$, $[M/H]$, and $[\alpha/M]$ values from our predictions and APOGEE labels. A Gaussian fit to the residuals is shown in the lower left inset of each plot.

2. Methods

- **Binary-star Model:**
- Assumes same age and composition for both components
- Parameter vector: $\theta_b = \{m_1, q, \log \tau, [M/H], [\alpha/M], v_{1,i}, \gamma\}$
- Secondary star RV calculated as $v_{2,i} = (\gamma \times (q + 1) - v_{1,i})/q$
- Requiring non-normalized spectra, which is a normalized single-star spectrum multiplied by the corresponding model-predicted pseudocontinuum created by Regli (B. Zhang 2019).
- Binary spectrum is a weighted combination: $F_h = f_1 \times R_1^2 \times \psi(q_{h, \text{mist}, 1}) + f_2 \times R_2^2 \times \psi(q_{b, \text{mist}, 2})$

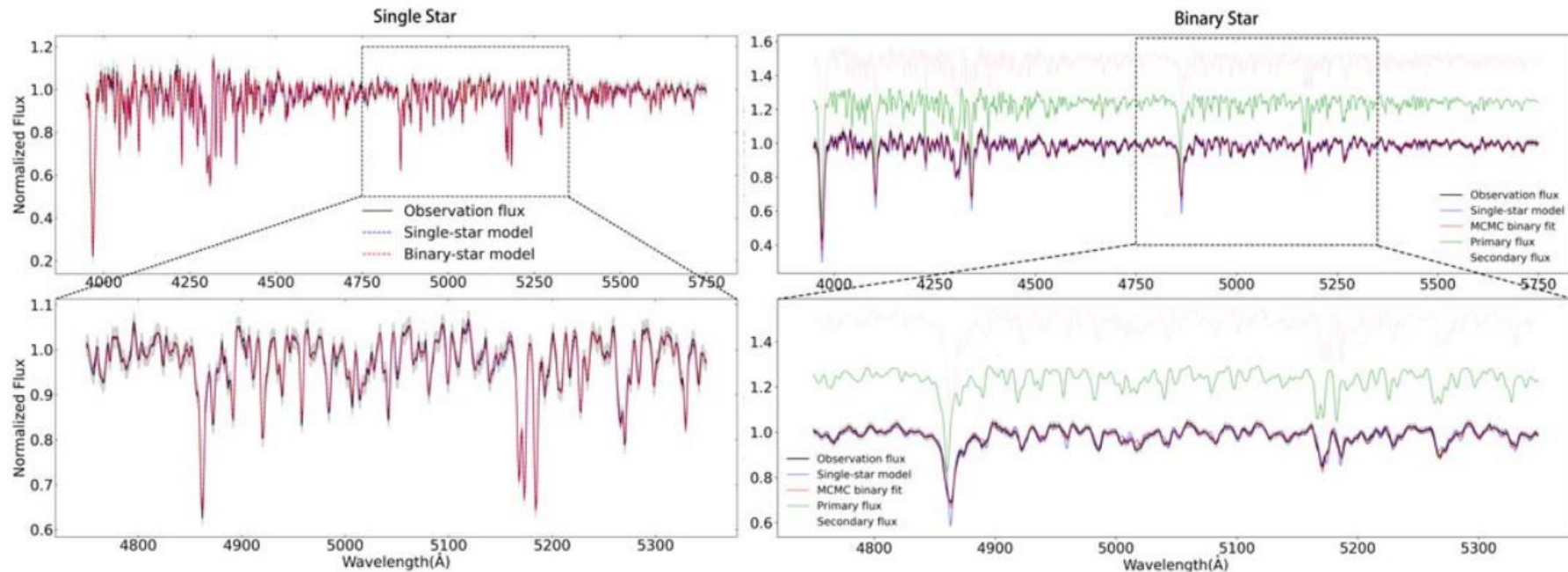


Figure 2. Comparing the spectral fittings with single-star (blue) and binary-star (red) models. The upper panels show the complete normalized spectra with the two best-fit models, while the lower panels illustrate the zoomed-in view of the spectra for a certain wavelength range. Left: both models show an almost identical fit to the spectrum. Right: The binary-star model fitting is significantly better than that of the single-star model. The spectra of the primary (pink) and secondary (green) stars are also shown.

2. Methods

- **Spectral Model Fitting:**

- SCIPY least_squares with "Trust Region Reflective" algorithm (M. A. Branch et al. 1999)
- Binary identification threshold: $\Delta\chi^2 = \chi^2_s - \chi^2_b > 0.4$

- **Binary Detection Criteria:**

- Optimal for high mass ratio systems ($q \geq 0.7$)
- Requires large velocity separation ($\Delta RV > 100$ km/s)
- Completeness reaches $\sim 45\%$ at $q \approx 0.95$

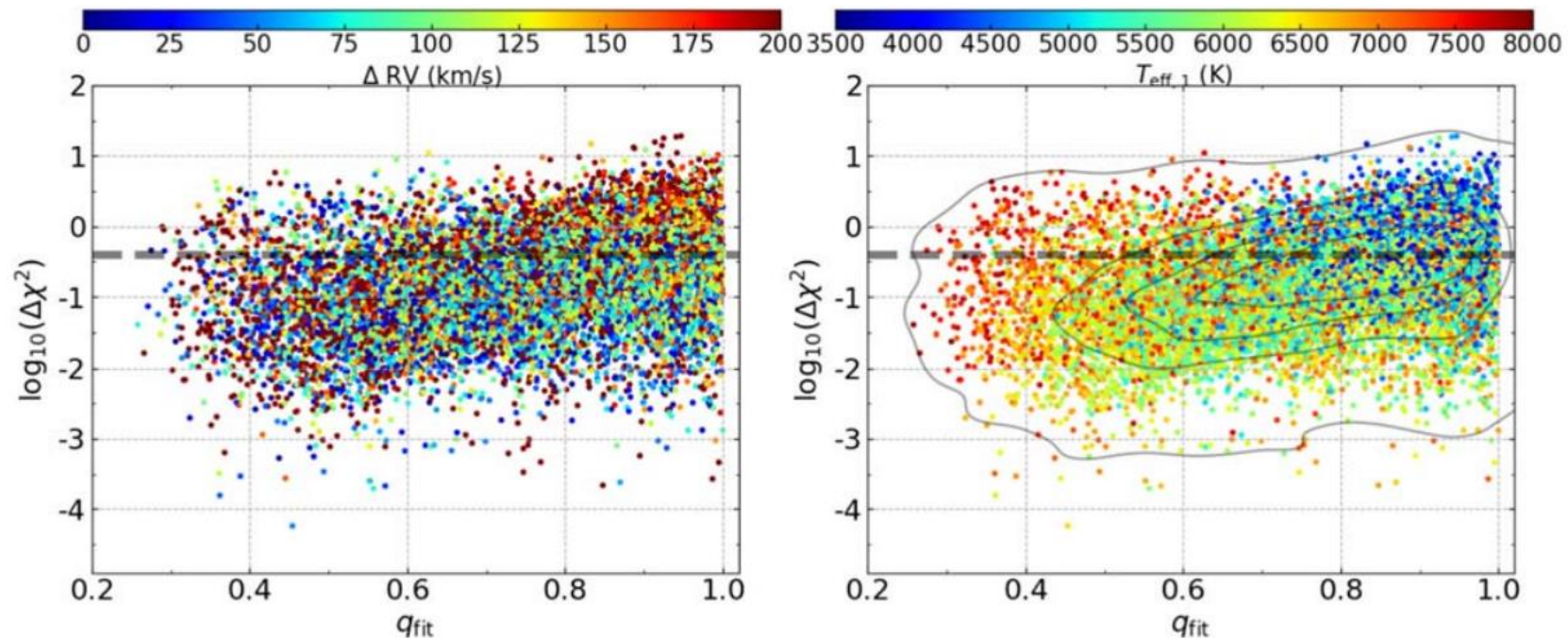


Figure 6. The q vs. $\log(\Delta\chi^2)$ from the results of single-star and binary-star model fitting for the semiempirical binary spectra. The color bar on the left is the RV offset ΔRV between the two components, and the one on the right is the temperature of the primary star. The dashed lines locate at $\log(\Delta\chi^2) = -0.4$. The black contour lines in the right panel represent the relative density of the data points. The closer to the inner rings, the higher the density of the data points.

2. Methods

- **Model Fitting and Uncertainty:**
- Combining spectral and photometric data: Spectroscopic data (LAMOST spectra), Photometric data (Gaia DR3 & 2MASS bands), Astrometric data (Gaia DR3 parallax) and Galactic extinction (dustmaps) and Using `emcee` package to fit and constrain the stellar parameters
- The fitting results of J0913 demonstrate the model can fit the spectra well in every phase, and the MCMC method effectively constrains various parameters.

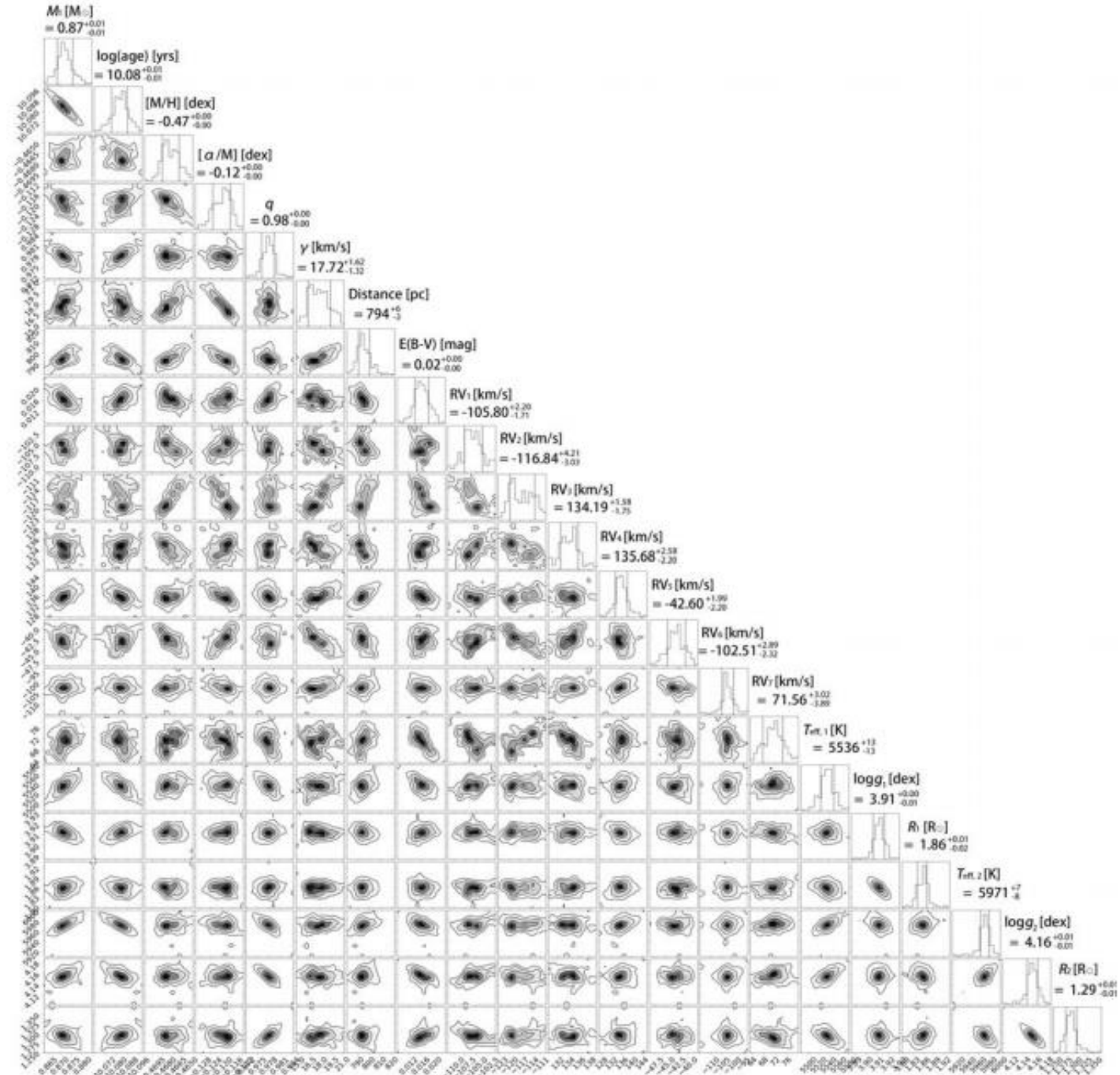


Figure 12. The marginalized posterior probability distributions from the MCMC fitting for J0913 with seven observational epochs (with RV values for the primary component). The parameter values are the median of the one-dimensional distributions, while the vertical dashed lines are located at the 16th and 84th percentiles.

3. Method Performance

- **RV Standard Star Fitting:**
 - 3,239 RV standard stars from APOGEE tested
 - No false positives using $\Delta\chi^2 > 0.4$ threshold
- **Mock Single-star Spectral Fitting:**
 - 10,000 mock single-star spectra tested
 - False positive rate: 2.3% at $\Delta\chi^2 > 0.4$ threshold
- **Confusion Matrix:**
 - Precision: 92.6%
 - Recall: 23.0%
 - Accuracy: 63.4%

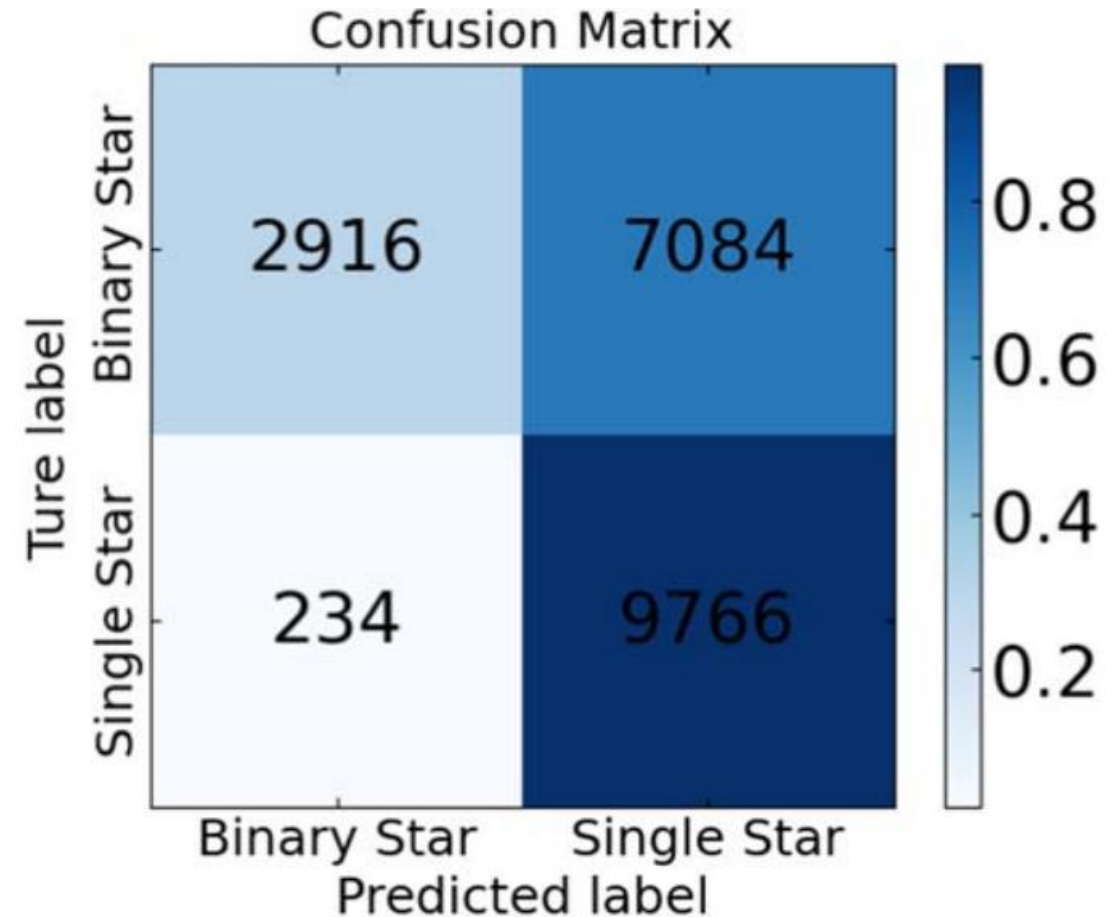


Figure 14. Confusion matrix of the model on the testing set. In the order of top to bottom, left to right, they represent TP, FP, FN, and TN, respectively.

4. Results and Cross Validation

- **SB2 Candidates and the Parameters:**

- **4,848** SB2 candidates identified from 3,584,214 LAMOST spectra

- Stellar parameters in the range of $4000 \text{ K} \leq T_{\text{eff}} \leq 7000 \text{ K}$, $3.5 \leq \log g \leq 5.0$, $-2.0 \leq [M/H] \leq 0.5$ and $-0.5 \leq [\alpha/M] \leq 0.5$; high mass ratio ($q > 0.9$), large RV separation

- **Multi-faceted Validation:**

- Color-Magnitude: Candidates positioned above main sequence

- Color-Temperature: Consistent with stellar evolution models

- Photometry: Binary model significantly better matches observed brightness

- Orbital Period: 96.6% agreement between spectroscopic and photometric periods

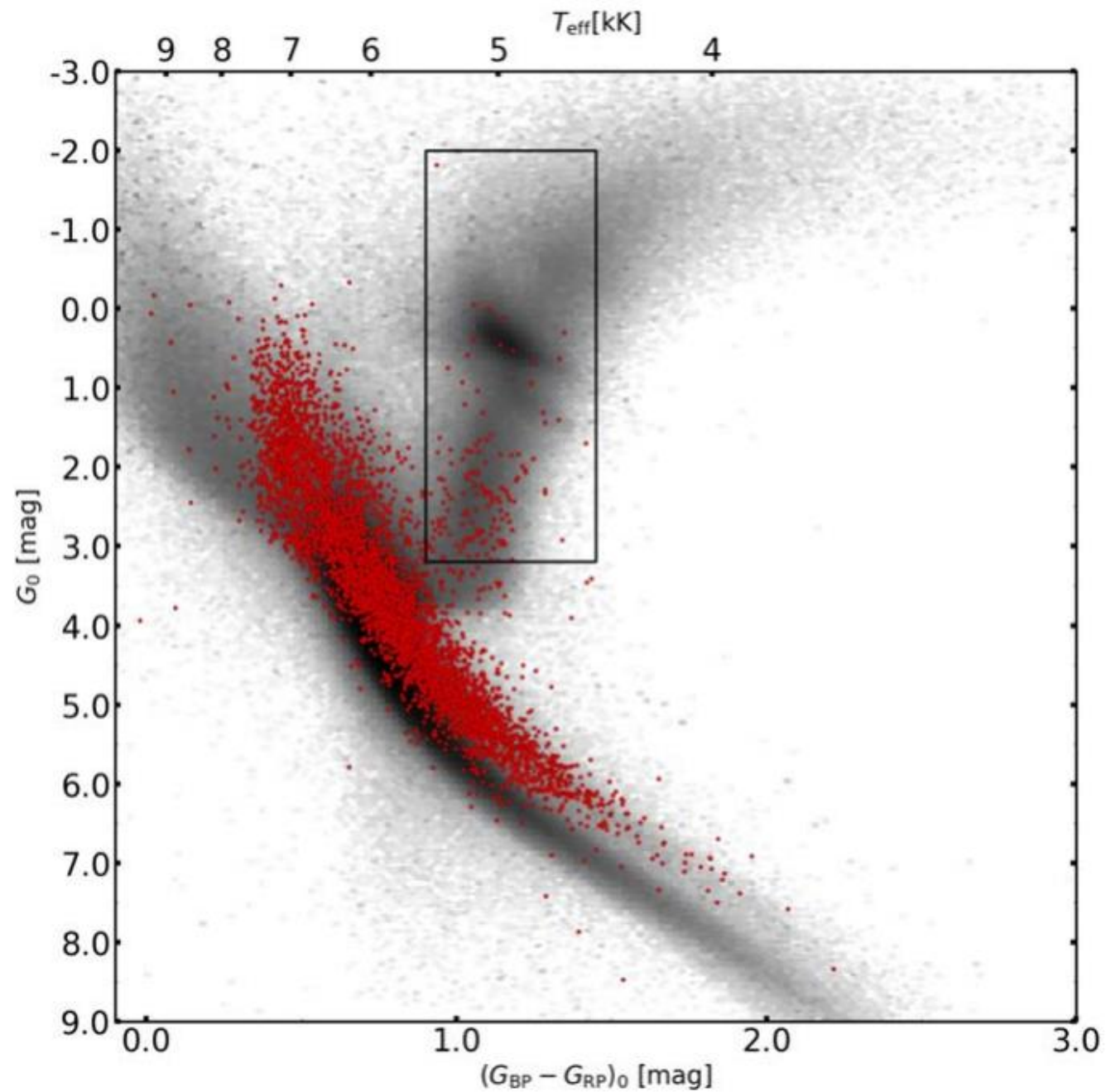


Figure 17. The CMD (red points) of the SB2 candidates found by this work. The black hot map shows the distribution of all LAMOST LRS DR9 objects after extinction correction. The black box indicates the region having binary candidates that include giant stars.

5. Comparison with Other Catalogs

- **ASAS-SN Validation:**
 - 2,596 candidates (53.5%) also identified as variables in ASAS-SN
 - 92.6% classified as eclipsing or ellipsoidal variables, confirming binary nature
 - Identified 19.9% of ASAS-SN eclipsing binaries
 - Non-detections mainly limited by mass ratio and RV separation constraints
- **Comparison with TESS:**
 - 408 common sources (8.42%)
- **Comparison with LAMOST Medium-resolution Survey:**
 - 231-455 common sources compared to 2318 binary candidates by [B. Zhang et al. \(2022\)](#) (depending on different criteria)
- **Comparison with APOGEE:**
 - 58 common sources
- **Comparison with Gaia DR3:**
 - 39 common sources (primarily short-period systems)
 - **This method excels at large RV separation (>100 km/s) and high mass ratio ($q \geq 0.7$) systems**

6. Summary

- In this work, the physical parameters provided for the identified 4848 binary-star candidates include not only atmospheric parameters such as effective temperature ($4000 \text{ K} \leq T_{\text{eff}} \leq 7000 \text{ K}$), surface gravity ($3.5 \leq \log g \leq 5.0$), and metallicity ($-2.0 \leq [M/H] \leq 0.5$) but also parameters like mass, radius, and age. In addition to spectral data, photometry, parallax, and extinction information are simultaneously fitted in the MCMC process. Therefore, we also present the distance and extinction parameters. The photometric magnitudes obtained from the binary-star model with the MIST are more consistent with the observed values than those from the single-star model, showcasing the validity of our SB2 identification method.
- Our results are primarily focused on main-sequence binary stars of FGK types (4713 objects). Additionally, there are 135 binary candidates with giant components. This property arises due to the skewed distribution of our training set. Nearly all of these candidates are located above the main sequence in the CMD, which suggests their binary nature. It is important to note that other types of binaries, such as white dwarf–main-sequence binaries and white dwarf–white dwarf binaries, are not investigated in this study.
- Given the LRS spectral resolution of $R \sim 1800$, our model exhibits favorable identification performance for sources with velocity differences exceeding 100 km s^{-1} , as inferred from semiempirical spectral experiments. This value is lower than the 50 km s^{-1} velocity resolution of the MRS. Due to the presence of numerous sources with high mass ratios in our sample, the assignment of radial velocities to incorrect member stars unavoidably occurs. In this study, we attempt to mitigate this problem by using a method of RV reversal to obtain the minimum $\chi^2_{\beta,e}$ value for the spectral fit. We provide $\delta\chi^2_{\beta,e}$ values before and after the RV inversion in the catalog to assess its impact on spectral fitting. Our model is well suited for cases with mass ratios $q \geq 0.7$. The completeness of the sample increases with the rise of the mass ratio, with a slight decline as it approaches 1.
- We provide orbital solutions for 44 short-period (≤ 10 days) objects with sufficient (≥ 7) observational epochs. Without performing additional RV swap, approximately 37.9% of the results are consistent with integer multiples of the periods provided by ASAS-SN. After performing further RV swap operations in RV curves fitting, the majority of the sources' RV period solutions can align with integer multiples of the photometric period.

Thanks!